

Finite element analysis of composite-to-steel type of joint for marine industry

Darko Burlović¹ · Arijana Milat¹ · Miloš Balunović¹ · Darko Frank¹ · Elias A. Kotsidis² · I. G. Kouloukouras² · Nicholas G. Tsouvalis²

Received: 7 October 2015 / Accepted: 6 April 2016 / Published online: 21 April 2016
© International Institute of Welding 2016

Abstract The usage of composite materials makes easier to form complex shapes with the advantage of reducing the weight of the ship. Moreover, composite material is not subject to corrosion, which is the major issue in a marine environment. This paper investigates the design of the adhesively bonded composite-to-steel joint for marine industry. One part of the joint is double-lap connection of steel plate and carbon fibre-reinforced plastics (CFRP), whereas the other part is a CFRP-skin sandwich panel with Divinycell® foam as the core. In order to simulate the behaviour of composite-to-steel joint, the finite element analysis is conducted. The results suggest that the analysed joint could be used in marine applications.

Keywords (IIW Thesaurus) Fibre reinforced composites · Finite element analysis · Structural reinforced composites · Dissimilar materials · Adhesive bonding

1 Introduction

The new SOLAS Regulation 17 (2002) contributed to the increased usage of the composite materials in the marine industry. According to the rules, construction with materials other than steel is allowed, provided that the safety level and non-combustibility is preserved. The advantages of the composites

are corrosion resistance, high durability, small weight, and good strength-to-weight ratio. These advantages allow composites to compete easily with other traditional building materials in the marine industry [1]. Fibre-Reinforced Plastic (FRP) applications are recently introduced in components of larger ships; the main reason for this being the demand for fast vessels in which, light weight is essential [2, 3]. One of such is the bow enclosure application found on container ships, bulk carriers, general cargo ships, etc. The bow enclosure is an application of a considerable size; see Fig. 1.

Its streamlined shape has the function to enhance the aerodynamic profile of the ship thus reducing air resistance as well as serving as protection from the seawater. Trends in the naval sector and the advantages that composite materials can offer make this application a future perspective to be explored.

This paper investigates the applicability of the connection of the composite bow enclosure with the pre-existing ship steel structure using the Finite Element (FE) analysis. Regarding joining composite substructures to the metal ship structures, adhesive or bolted joint, or the combination of these two are the most common options [4–10]. For the purpose of bow enclosure application, the bonded joint, comprising of a double-lap steel-to-carbon fibre plastic (CFRP) joint and a CFRP-skin sandwich with the Divinycell® core has been used. This type of joint is a modification of the composite-to-steel type of joint proposed by [9].

2 Application case

The idea of the composite bow enclosure is developed within the EU FP7 project “MOSAIC”. The bow enclosure made of steel is already used on some container ships and offshore supply vessels where it serves as a wave breaker. Due to the fact that steel is more difficult and expensive to form, the bow

Recommended for publication by Commission XVI - Polymer Joining and Adhesive Technology

✉ Darko Frank
darko.frank@as2con.com

¹ As2con-Alveus Ltd, Rijeka, Croatia

² National Technical University Of Athens, Athens, Greece

Fig. 1 Bow enclosure

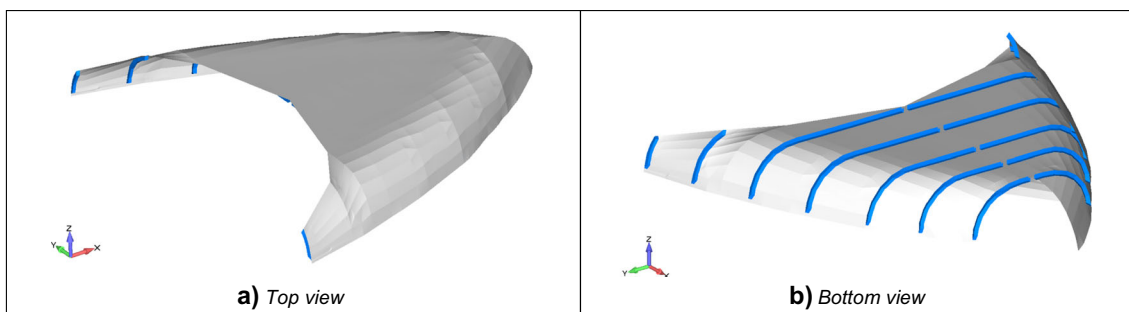


Fig. 2 Bow enclosure geometry

enclosure made of CFRP is investigated. The usage of CFRP makes easier to form complex shapes with the advantage of reducing the weight of the ship. Moreover, composites have good mechanical properties such as strength-to-weight and stiffness-to-weight ratios. The implementation of the

composite material to the bow enclosure is considered on the example of a 50.000 DWT Handymax tanker from EU FP7 project Ulysses [11]. The bow enclosure is 17.8 m long, 2.4 m high, and it is positioned above the main deck. Figure 2 shows the bow enclosure structure that is made of sandwich panels. The sandwich of the enclosure is made of a 100 mm thick Divinycell® H200 foam core and 6.8 mm thick CFRP skins on both sides, which in turn gives a total thickness of 113.6 mm. Each CFRP skin has 68 unidirectional fibres with the orientation 0/90/45/-45/30/60/120/150/0. CFRP skins consist of carbon fibres and Vinylester with the equal mass content. Mechanical properties of the materials are given in Tables 1 and 2.

Table 1 Carbon/Vinylester—mechanical properties [12]

Mechanical properties of carbon fibre/Vinylester (orthotropic elastic material)

Density	1500 kg/m ³		
Compressive modulus	$E_{11} = 111410 \text{ MPa}^a$	$E_{22} = 5619 \text{ MPa}$	$E_{33} = 5619 \text{ MPa}$
Poisson coefficient	$\nu_{12} = 0.279$	$\nu_{13} = 0.279$	$\nu_{32} = 0.279$
Shear modulus	$G_{12} = 3417 \text{ MPa}$	$G_{31} = 3417 \text{ MPa}$	$G_{23} = 2391 \text{ MPa}$
Tensile strength	$\sigma_{1T} = 1337 \text{ MPa}^b$	$\sigma_{2T} = 48 \text{ MPa}$	$\sigma_{3T} = 48 \text{ MPa}$
Compressive strength	$\sigma_{1C} = 947 \text{ MPa}$	$\sigma_{2C} = 129 \text{ MPa}$	$\sigma_{3C} = 129 \text{ MPa}$
Shear strength	$\tau_{12} = 55 \text{ MPa}$	$\tau_{13} = 55 \text{ MPa}$	$\tau_{32} = 55 \text{ MPa}$

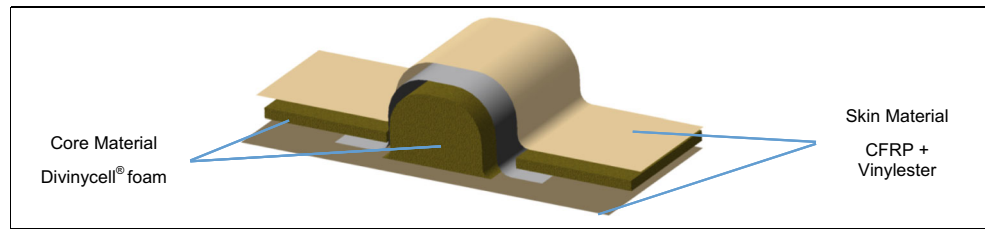
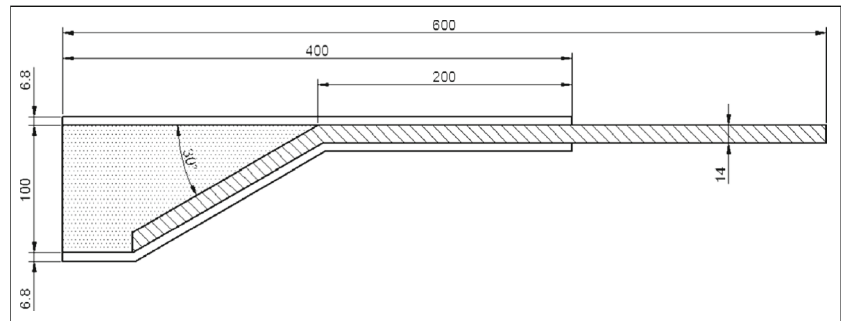
^a Direction of axis 1 corresponds to direction of glass fibre, direction of axis 2 is in plane with fibre and perpendicular to direction of axis 1, while the direction of axis 3 is defined as the normal to the surface of the fibre

^b Index T indicates critical tensile strength, and index C indicates critical compressive strength

Table 2 Core properties

Mechanical properties of Divinycell® foam [13]

	Units	H200
Density	kg/m ³	200
Compressive modulus	MPa	310
Poisson coefficient	–	0.4
Shear modulus	MPa	73
Tensile strength	MPa	7.1
Compressive strength	MPa	5.4
Shear strength	MPa	3.5

Fig. 3 Reinforcement geometry**Fig. 4** Joint scantlings

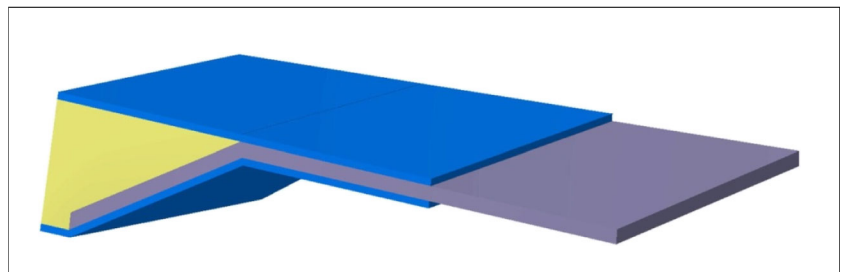
Transversal reinforcements with thicker core were added to stiffen the enclosure at the locations of the ship web frames. The reinforcements are marked blue in Fig. 2, whereas Fig. 3 shows the detail of the reinforcement.

The structure of the bow enclosure is connected to the steel structure by the composite-to-steel type of joint. The geometry of composite-to-steel joint used for the bow enclosure application is a slightly modified geometry presented in Kotsidis et al. [9]. It is an adhesively bonded butt-joint, comprised of a double-lap steel-CFRP joint and a CFRP sandwich composite part. The numerical study in the Kotsidis et al. [9] investigated the influence of various design parameters on the mechanical behaviour of a composite-to-steel joint under tensile and bending loads. The results showed that some design parameters can improve the joint's strength and stiffness and accordingly, the selected parameters suited for this paper are adjusted for the bow enclosure application. The joint parameters are given in Fig. 4.

The CFRP skins are adhesively bonded by Vinylester to AH36 steel and core material in a way shown in Fig. 5. Steel is depicted with grey colour; sandwich skins (CFRP) are marked with blue, whereas the core (Divinycell® foam) is coloured yellow. The joint has 200 mm overlap between the steel and CFRP and 30 degrees inclination of the steel plate towards the sandwich part; Fig. 4. The geometry of the joint has a slightly curved surface as it follows the bow design.

3 Finite element analysis

The finite element analysis in NX NASTRAN is conducted in order to validate the bow enclosure and the joint between the composite and the steel structure. During the course of the investigation the impact of the wave pressure is considered according to The Rules [14]. The composite structure has been modelled using four node laminate plates, but the core material of transversal reinforcements has been modelled using

Fig. 5 Joint detail

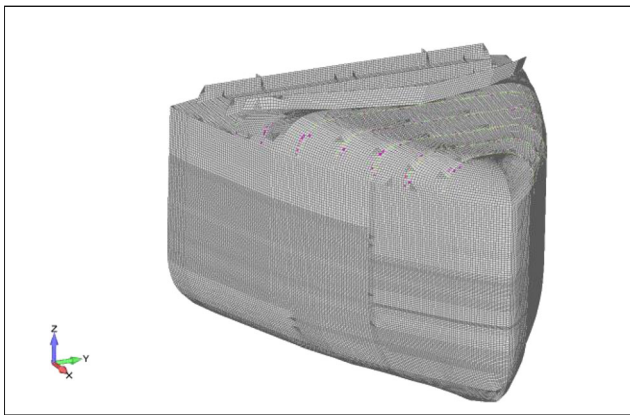


Fig. 6 FE model of ship's bow with the bow enclosure

eight node solid elements because of the large thickness-to-length ratio; Fig. 3. The average element size was 200 mm. Figures 6 and 7 represent the global FE model which includes the steel bow of a 60000 DWT Handymax tanker and a composite bow enclosure, while Fig. 7 shows the bow enclosure alongside the transverse reinforcements and supporting pillars. For the material modelling, steel was considered as isotropic, elastic-plastic material with bilinear isotropic hardening, whereas composite and core materials were considered as homogenous, linear elastic orthotropic material.

All translations and rotations are suppressed at the nodes on the aft end of the model. These nodes are presented in red colour in Fig. 8. In the same figure, the elements where the seawater pressure is applied are marked yellow.

The major problem of implementing composite structures to conventional steel ships is connecting these materials together. The FE model in Figs. 6, 7, and 8 was used to study the bow enclosure without taking into account the influence of the composite-to-steel joint. Therefore, the fine mesh model is used to investigate the local stress levels of the joint. For this purpose, the detail with the highest stresses in the composite-to-steel interface was analysed in ANSYS 13 [15]. Figure 9 shows the location of the highest stress levels along the interface within the bow enclosure model, which is further analysed in the form of a local submodel is shown in Fig. 10.

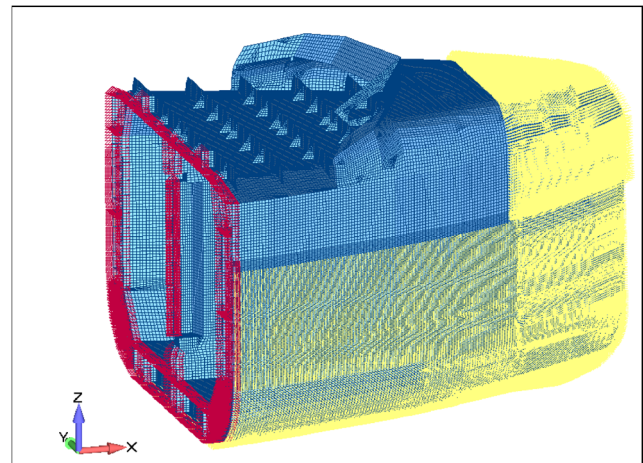


Fig. 8 Boundary conditions and loads

The average element size of 6 mm was used for the joint model (Fig. 11). All materials were modelled using eight node solid elements (SOLID185). Moreover, the elements used for CFRP skins were layered solids (SOLID185) in order to model the different orientations of the carbon layers. The nodal displacements obtained from the bow enclosure analysis are mapped to the model of the joint using the “shell to solid” option in ANSYS. This option applies the translations to the solid element nodes and also the rotations from the shell nodes in a way that it imposes the planar rotation to the multiple solid nodes at locations where only one shell-node existed in the bow enclosure model.

If the actual adhesive law is not available from the test data, the adhesives can be modelled with the elastic law. This assumption is justified by the fact that this law fits quite well the behaviour of the rigid adhesive and the resin commonly used to bond the patch.

The possibility of debonding between different material interfaces was investigated using the cohesive zone model. This method uses contact elements and in this case, TARGE170 and CONTA174 elements are used as contact pair. The contact is defined between three interfaces: CFRP-steel, CFRP-core, and steel-core. The cohesive properties are implemented through the triangular cohesive law.

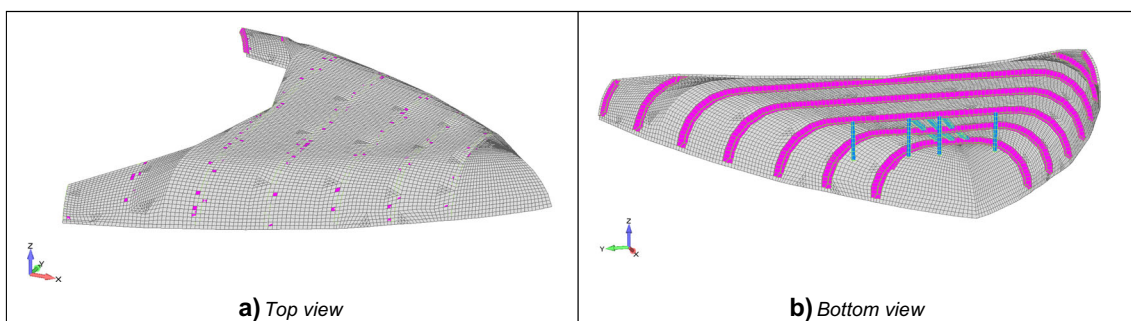


Fig. 7 FE model of the bow enclosure

Fig. 9 Location of the highest stresses along the joint

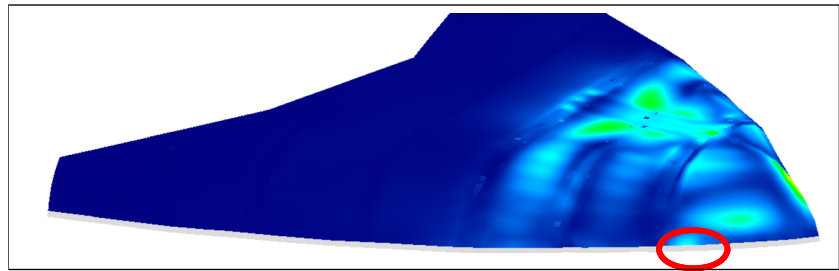


Fig. 10 Position of the sub model

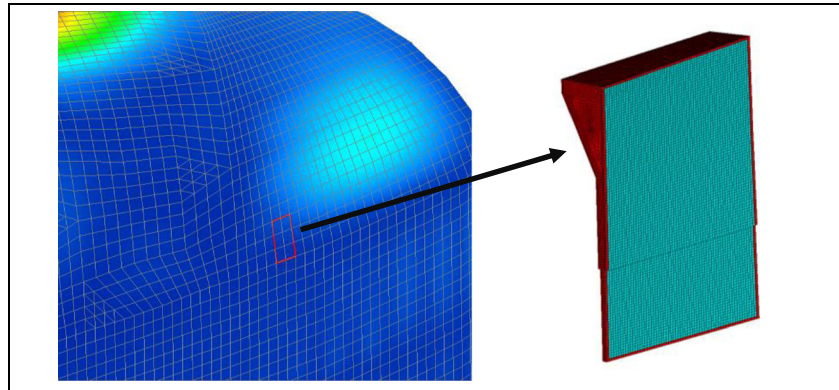
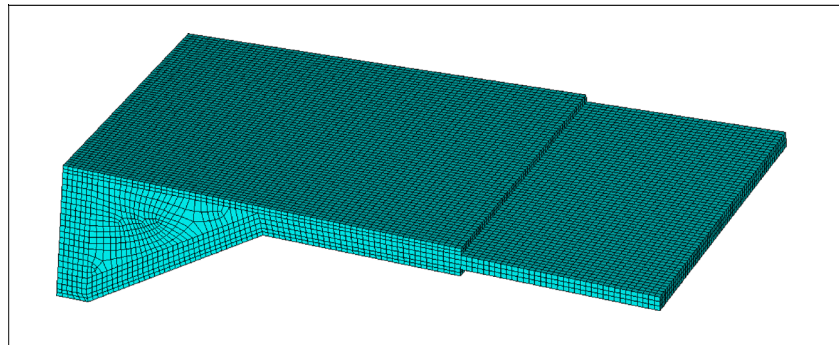


Fig. 11 Fine mesh model of the joint



The adhesive material is Vinylester which was also used as the resin for the sandwich skin, as described in Chapter 2. The material properties of Vinylester resin are taken from EU FP7 Project CO-PATCH [12] and given in Table 3. These cohesive

properties are based on the experimental results obtained within the scope of the project and are given here in Table 4. The thickness of the cohesive elements is taken as zero according to the CO-PATCH [12].

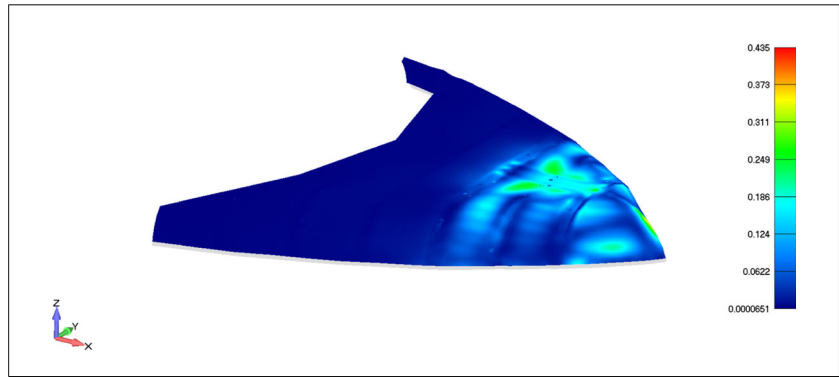
Table 3 Adhesive/resin properties

Mechanical properties of Vinylester resin [12]		
	Units	Vinylester
Young’s modulus	MPa	3350
Poisson coefficient	–	0.26
Tensile breaking stress	MPa	75
Tensile breaking strain	%	2.2

Table 4 Cohesive properties [12, 16]

	Mode I (normal direction)	Mode II (tangential direction)
Maximum stress	82.5 MPa	82.5 MPa
Maximum gap	0.0027	0.0027
Contact stiffness	40740 MPa	

Fig. 12 Tsai-Hill failure index—bow enclosure



4 Results

The response in a form of Tsai-Hill [17] failure index is shown in Fig. 12 for the bow enclosure model. The maximum failure index is 0.426, which is far below the limit of 1, and therefore, the structure seems to be safe from the impact of the sea pressure.

Tsai-Hill criterion takes account of interactions between failure modes and mostly is an adaptation of von Mises criterion adjusted for anisotropic materials. Failure occurs if the inequality is violated:

$$\left(\frac{\sigma_1}{\sigma_{1u}}\right)^2 + \left(\frac{\sigma_2}{\sigma_{2u}}\right)^2 - \frac{\sigma_1\sigma_2}{\sigma_{1u}^2} + \left(\frac{\tau_{12}}{\tau_{12u}}\right)^2 \leq 1$$

Where σ_1 , σ_2 , and τ_{12} are normal and shear stresses in the composite. σ denotes tensile stress and τ denotes shear stress. Index 1 corresponds to the direction of the composite fibre and index 2 corresponds to the direction in the plane of the fibre. Index u indicates critical strength in the composite and the values are taken from Table 1. If the values of σ_1 and σ_2 are positive, the σ_{1u} and σ_{2u} are tensile strengths. If the values of σ_1 and σ_2 are negative, the σ_{1u} and σ_{2u} are compressive strengths.

However, the main concern is the interface between the composite and the steel structure. Figure 13 presents the displacements of the joint model. The remaining Figs. 14, 15, 16, 17, and 18 omit the elements close to the boundary conditions in order to exclude the unrealistic stress concentrations.

The highest occurring stresses in the steel are shown in Figs. 14 and 15. Considering the small edge element length, the obtained stress is well within permissible limit. Maximum permissible stress for fine mesh analysis is calculated according to the yield utilisation factor λ_y . For this particular case the permissible stress range is given by the expression $\lambda_y \leq 1.7$ (The Rules [14], Sec. 9/2.3.5).

The permissible stress limit (grade AH36 steel) for mesh size of 50×50 mm is calculated by:

$$\sigma_{vm} = \frac{\lambda_y \cdot 235}{k} = \frac{1.7 \cdot 235}{0.72} = 555 \text{ MPa}$$

Where σ_{vm} is the von Mises stress calculated at element’s centroid.

Furthermore, Tsai-Wu failure criterion [18] was investigated for the core and skins and in the both cases, the index was less than the critical value of 1; see Figs. 16 and 17.

Fig. 13 Total displacement [mm]—deformed model

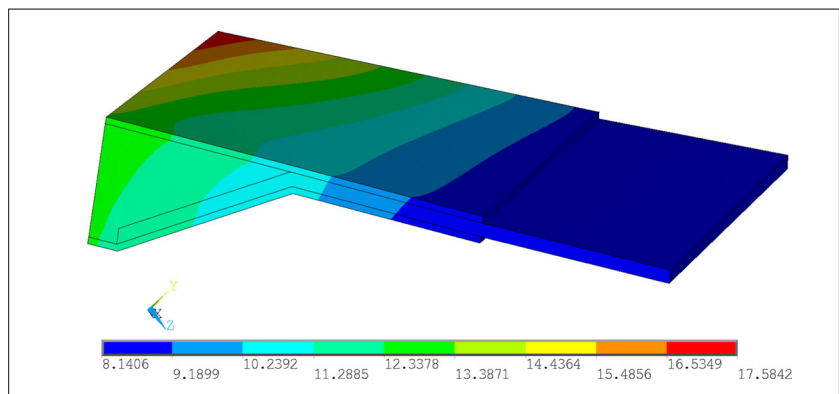


Fig. 14 Von Mises stresses calculated from element centroid in AH36 steel [MPa]—top view

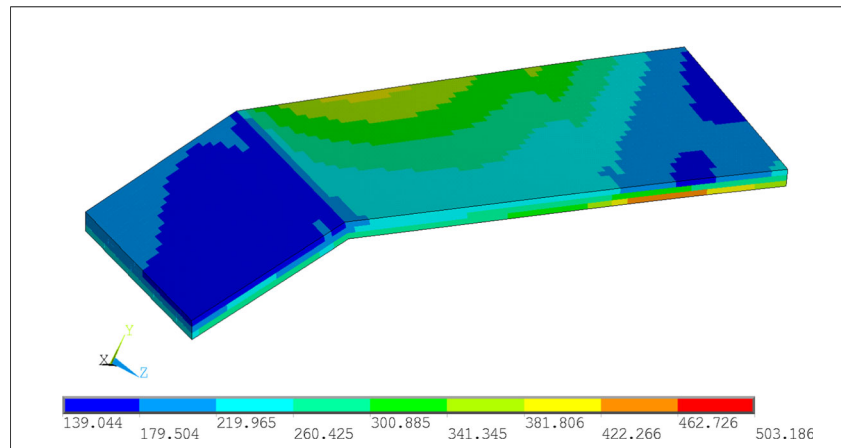
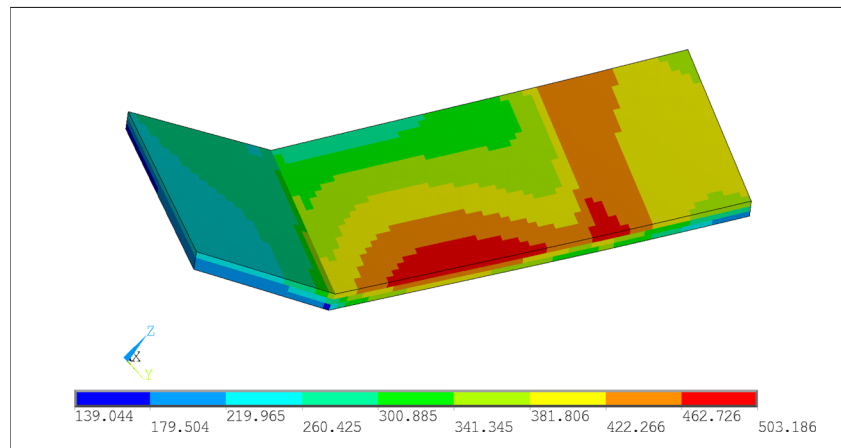


Fig. 15 Von Mises stresses calculated from element centroid in AH36 steel [MPa]—bottom view



The results also showed that, according to FE results, there is no danger of debonding between different materials; see contact total stress (CTS) plots for all three interfaces in Fig. 18. The CTS is the vector sum of normal and tangential contact stresses that gives the permissible CTS of 116.68 MPa resulting from the values given in Table 4. The stresses that occur in contact elements between all three interfaces are below this permissible limit of

116.68 MPa. The maximum total contact stress in the interfaces between the composite and core material, core and steel, and composite and steel material are equal to 48.6, 48.8, and 105.7 MPa, respectively. Phenomena such as creeping and temperature effects are not considered in the present study. Displacement distribution in the joint sub model corresponds to the applied mapped translations and rotations from the global model, as shown in Fig. 13.

Fig. 16 Tsai-Wu failure criteria in CFRP composite material—results from the layer with maximum value

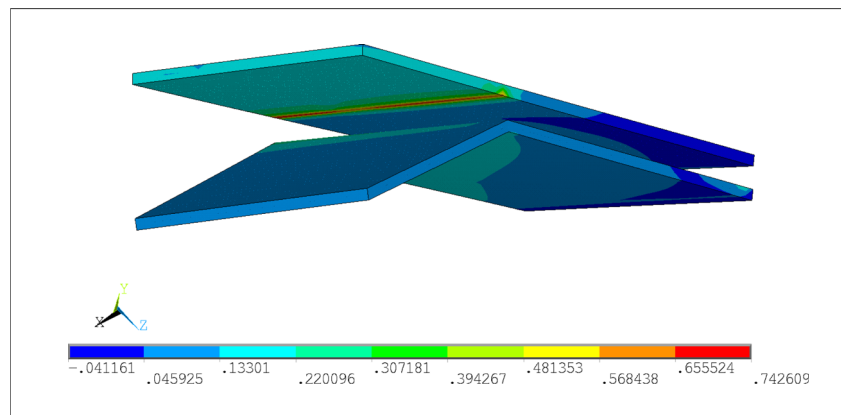
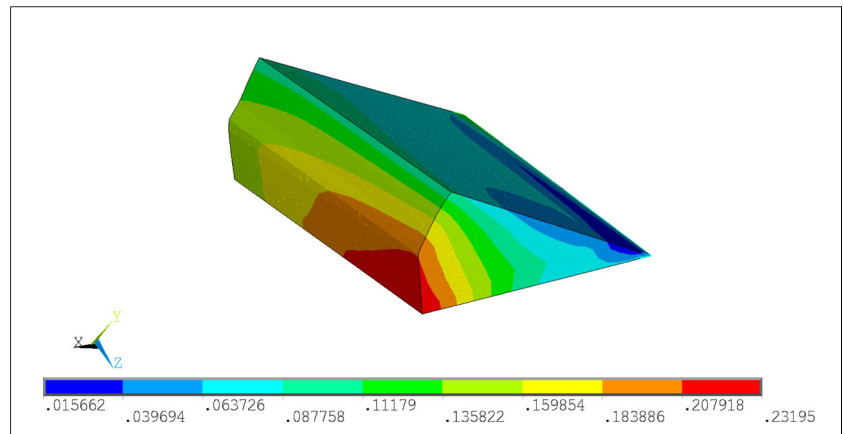


Fig. 17 Tsai-Wu failure criteria in Divinycell® core material



Considerable stress appears in the steel part, especially on the inner side of the plate, but within permissible limits. See Figs. 14 and 15.

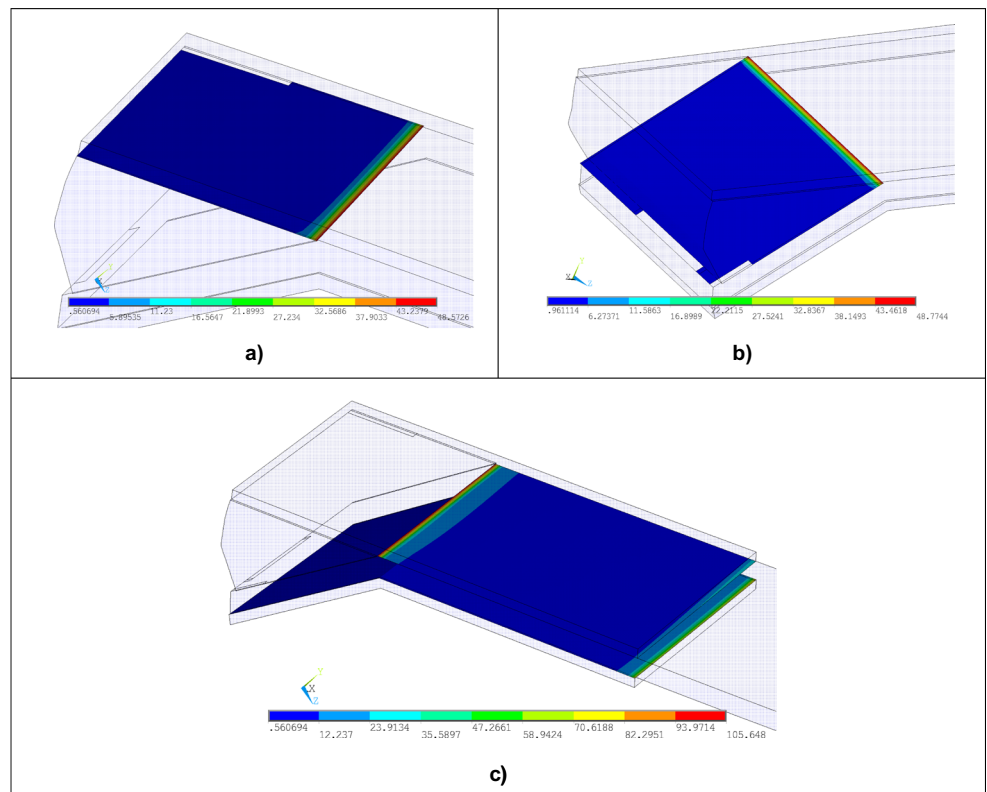
The highest value of failure criteria index in the composite part is located around the edge where the sandwich skin, core, and steel part are joined; see Fig. 16. At this location also the highest contact stresses occur; see Fig. 18. These results suggest that the alternative version of the joint should also be considered, for example, in a form of the curved design in order to create more even stress distribution over the adhesive joint.

The core material itself shows lower failure index than the sandwich skin, as seen in Fig. 17.

5 Conclusion

This paper aimed to investigate the design of the adhesively bonded composite-to-steel type of joint and its applicability in marine industry. The joint comprises of double-lap connection of steel plate and carbon fibre reinforced plastics (CFRP) at one side, whereas the other side is the CFRP-skin sandwich panel with Divinycell® foam as the core. The investigation considered the application case of the composite bow enclosure, which has to withstand the loading of the seawater in rough seas. In order to simulate the behaviour of composite-to-steel joint, the finite element analysis employed the two-stage analysis. Firstly, the global response of the bow

Fig. 18 Contact total stress [MPa]; **a** composite-core interface; **b** core-steel interface; **c** composite-to-steel interface



enclosure was obtained. Then, the displacements from the global analysis were mapped to the local FE model of the joint. The analysis of the joint uncovered that the stress levels are within the permissible limits and that there is no danger of debonding between the materials. These results suggest that the joint is potentially applicable in the marine industry as already proposed by [9]. However, the phenomena like creeping and temperature dependence have not been taken into account within the scope of the study. Therefore, the future work should consider creeping, temperature, and a curved design of the joint. In addition, mechanical tests should be performed before the industrial application of the joint.

Acknowledgements MOSAIC is the acronym for the “Materials On-board: Steel Advancement and Integrated Composites”, a project supported by the European Commission under the FP7-SST-2012-RTD-1 Sustainable Surface Transport programme. The support is given under the scheme of RTD, Grant Agreement No. 314037.

References

1. Lesani M, Bahaari MR, Shokrieh MM (2014) Experimental investigation of FRP-strengthened tubular T-joints under axial compressive loads. *Constr Build Mater* 53:243–252
2. Baker A (1984) Repair of cracked or defective metallic aircraft components with advanced fibre composites - an overview of Australian work. *Compos Struct* 12:153–181
3. Baker A, Cheste R, Davis M, Roberts J, Retchford J (1993) Reinforcement of the F-111 wing pivot fitting with a boron/epoxy doubler system-materials engineering aspects. *Composites* 24:511–521
4. Boyd SW, Blake JIR, Shenoi RA, Kapadia A (2004) Integrity of hybrid steel-to-composite joints for marine application. *Proceedings of the Institution of Mechanical Engineers Part M: J. Engineering for the Maritime Environment* 218(4):891–906
5. Boyd SW, Blake JIR, Shenoi RA, Mawella J (2008) Optimization of steel-composite connections for structural marine applications. *Composites: part B* 39:891–906
6. Cao J, Grenestedt JL (2003) Test of a redesigned glass-fibre reinforced vinyl ester to steel joint for use between a naval GRP superstructures and a steel hull. *Compos Struct* 60:439–445
7. Clifford SM, Manger CIC, Clyne TW (2002) Characterization of a glass-fibre reinforced Vinylester to steel joint for use between a naval GRP superstructure and a steel hull. *Compos Struct* 57(1–4):50–66
8. Hentinen M, Hildebrand M, Maunu V. (1997) Adhesively bonded joints between FRP sandwich and metal. ESPOO Technical Research Centre of Finland, VTT Tiedotteita - Meddelanden - Research Notes 1862:44
9. Kotsidis EA, Kouloukouras IG, Tsouvalis NG (2014) Finite element parametric study of a composite-to-steel-joint. *Maritime Technology and Engineering*, 627–635
10. Wright PNH, Wu Y, Gibson AG (2000) Fibre reinforced composite-steel connections for transverse ship bulkhead. *Plastics, Rubber and Composites: Processing and Applications*, PRC, Institute Materials 29(10):549–557
11. EU FP7 Project: ULYSSES - Ultra Slow Ships (2013). Deliverable 5.2: Structures - results of Phase II - The 2020 ship
12. CO-PATCH EU FP7 Project—composite patch repair for marine and civil engineering infrastructure applications, “D4.4.2 Report with the numerical modeling guidelines - Final issue”. (2012)
13. THE DIAB GROUP. Divinycell® H Technical Data. <http://www.diabgroup.com/> Laholm, Sweden, 2012
14. IACS Common structural rules for double hull oil tankers with length 150 meters and above. (July 2012)
15. ANSYS Inc., (2010) *ANSYS 13 Help*, Canonsburg, PA, USA
16. The Focus, PADT, A Publication for ANSYS Users. Issue 56, www.padtinc.com (April 2007)
17. Tsai SW (1965) Strength characteristics of composite materials NASA-CR 224. National Aeronautics and Space Agency, Washington, DC
18. Tsai, S. W; Wu, E. M. (1971) A general theory of strength for anisotropic materials. *J Compos Mater (NASA CR-224)* 5:58–80